The Canadian Mineralogist
Vol. 37, pp. 207-221 (1999)

EFFECTS OF DOSE RATE AND TEMPERATURE ON THE CRYSTALLINE-TO-METAMICT TRANSFORMATION IN THE ABO_4 ORTHOSILICATES

ALKIVIATHES MELDRUM[1], LYNN A. BOATNER AND STEVE J. ZINKLE

Oak Ridge National Laboratory, Oak Ridge, Tennessee 37831-6057, U.S.A.

SHI-XIN WANG, LU-MIN WANG AND RODNEY C. EWING

Department of Nuclear Engineering and Radiological Sciences and Department of Geological Sciences, The University of Michigan, Ann Arbor, Michigan 48109, U.S.A.

ABSTRACT

Displacive radiation-induced effects that accumulate during geological time in the uranium- and thorium-bearing orthosilicate minerals zircon, hafnon, thorite, and huttonite were investigated by ion-bombardment techniques and compared with radiation-damaged natural specimens. The atomic-scale changes in microstructure that occur with increasing dose of radiation are similar in both cases, but a polycrystalline microstructure occurs in the natural minerals that has only been found in synthetic specimens irradiated at elevated temperature. For ion-beam-irradiated synthetic crystals and natural crystalline thorite from the Kipawa complex, western Quebec, the dose required for amorphization increases with increasing temperature. At temperatures above 600°C, the amorphization dose increases in the order: Kipawa thorite, synthetic thorite, hafnon, zircon and huttonite. The synthetic polymorphs of $ThSiO_4$ require a similar dose for amorphization at temperatures below 500°C; thus huttonite is not intrinsically more radiation-damage-resistant than thorite. Rather, huttonite recrystallizes more rapidly at elevated temperatures. The temperature above which amorphization cannot be induced by α-decay processes was calculated by further developing and applying a recently derived model that can also predict the transformation from the crystalline to metamict state in zircon as a function of age and temperature. The model was refined and expanded to include thorite and huttonite.

Keywords: zircon, hafnon, thorite, huttonite, metamict state, amorphization, irradiation.

SOMMAIRE

Les déplacements d'atomes dus à la radiation accumulée au cours des temps dans les orthosilicates zircon, hafnon, thorite et huttonite porteurs d'uranium et de thorium ont été étudiés par bombardement ionique. Les résultats sont comparés avec des échantillons naturels endommagés par la radiation. Les changements microstructuraux à l'échelle atomique qui résultent d'une augmentation de la dose de radiation sont semblables dans les deux cas, mais une microstructure polycristalline dans les minéraux naturels se voit dans les échantillons synthétiques seulement s'ils ont été irradiés à température élevée. Dans le cas d'échantillons synthétiques et d'un échantillon de thorite du complexe de Kipawa, dans l'ouest du Québec, bombardés avec un faisceau ionique, la dose requise pour l'amorphisation augmente à mesure qu'augmente la température. Au dessus de 600°C, la dose requise pour l'amorphisation augmente dans l'ordre: thorite de Kipawa, thorite synthétique, hafnon, zircon et huttonite. Les polymorphes synthétiques de $ThSiO_4$ requierrent une dose semblable pour assurer l'amorphisation en dessous de 500°C; il ne semblerait donc pas que la huttonite possède une résistance intrinsèque plus grande à la radiation que la thorite. En revanche, la huttonite peut recristalliser plus rapidement à température élevée. La température au delà de laquelle une amorphisation n'est plus possible par processus de bombardement de particules α a été calculée en affinant un modèle récemment développé; celui-ci permet aussi de prédire la transformation de l'état cristallin à l'état métamicte dans le zircon en fonction de l'âge et de la température. Le modèle a de plus été affiné et augmenté pour inclure la thorite et la huttonite.

(Traduit par la Rédaction)

Mots-clés: zircon, hafnon, thorite, huttonite, état métamicte, amorphisation, irradiation.

[1] *E-mail address*: al-m@worldnet.att.net

Introduction

The study of radiation-damaged minerals goes back over a century to Jacob Berzelius's systematic investigations of the "pyrognomic" properties of metamict gadolinite (Berzelius 1815). In the late 19th century, W.C. Brøgger coined the term "metamikt" to describe originally crystalline materials which had, over the course of time, assumed the properties of an amorphous substance (Brøgger 1890). Although the critical role of radiation was not noted by Brøgger (radioactivity was not discovered until 1896), the metamict state is now considered to be a radiation-induced transformation from the periodic to the aperiodic state (Ewing 1993). Thus ion-beam irradiation techniques can be used to simulate and study the process of metamictization under well-controlled conditions of irradiation. Because of its widespread use for U–Pb geochronology (*e.g.*, Krogh & Davis 1975, Krogh 1982, Heaman & Parrish 1991), zircon ($ZrSiO_4$) is a mineral for which ion-beam irradiations have been used to simulate α-decay damage (Wang & Ewing 1992a, b). Zircon becomes metamict after receiving a cumulative dose of approximately 10^{16} α-decays/mg (Holland & Gottfried 1955, Murakami *et al.* 1991, Weber *et al.* 1994). Each α-decay produces a high-energy (4–6 MeV) α-particle and a low energy (~100 keV) recoil nucleus. Most of the actual damage, in terms of the total number of atomic displacements, is caused by the more massive recoil nucleus. The number of displaced atoms produced by each α-decay event depends linearly on the atomic displacement energies (E_d), defined as the energy necessary to permanently displace an atom from its lattice site (see Table 1 for a list of symbols used in the present work). For zircon, the E_d values have been recently estimated to be 73 eV for Zr, 47 eV for Si, and 23 eV for O (Weber *et al.* 1998). Using these new values, a 5 MeV α-decay in zircon produces approximately 800 atomic displacements.

The microstructural effects of radiation damage can be measured using a variety of techniques. Transmission electron microscopy (TEM) is a particularly useful tool for radiation-damage studies because the microstructure can be directly observed on the atomic scale, the local chemical composition can be obtained by energy-dispersion X-ray spectrometry (EDS) techniques, and the relative amount of amorphous material can be estimated by electron diffraction. An electron microscope may also be interfaced to an ion accelerator so that materials may be irradiated over a range of temperature *in situ* in the TEM. Investigations of this kind have been reported for the cases of zircon (Wang & Ewing 1992a, b, Weber *et al.* 1994), apatite (Wang *et al.* 1994), monazite (Meldrum *et al.* 1997a), pyrochlore (Wang *et al.* 1999), and a group of SiO_2–Al_2O_3–MgO minerals (Wang 1997). This technique allows the researcher to directly observe the transformation from the crystalline to the amorphous state as a function of increasing ion dose at temperatures ranging from –250 to 850°C. Experimentally controllable variables include the type of ion (zircon has been irradiated with ions ranging in mass from He to Bi: Weber *et al.* 1999), ion energy, flux (*i.e.*, dose rate), and temperature. Synthetic crystals may be used in cases where natural specimens are not available (*e.g.*, hafnon and huttonite in the present study) and in order to eliminate the effect of impurities as a source of experimental error. The damage accumulation for ion-beam-irradiated synthetic single-crystal specimens and for naturally α-decay-damaged specimens can be directly compared in the TEM.

In a previous study, the microstructural evolution with increasing dose of radiation was found to be the same for single-crystal zircon irradiated by 1500 keV Kr^+ ions and for 550 Ma, α-decay-damaged zircon from Sri Lanka (Weber *et al.* 1994). Despite the large difference in dose rate (approximately 14 orders of magnitude) and the possibility of long-term annealing processes that may occur over geological time, the total dose for amorphization measured in units of displacements per atom (dpa) was determined to be approximately the same for the two cases (Weber 1990, Weber *et al.* 1994). In contrast, direct evidence was obtained for long-term annealing of radiation damage in natural zirconolite and zircon (Lumpkin & Ewing 1988, Lumpkin *et al.* 1994, 1998). The 550 Ma Sri Lanka zircon should, therefore, require a *higher* dose to become metamict owing to long-term annealing processes.

In the present study, we compare the microstructural evolution of synthetic zircon irradiated with 800 keV Kr^+ ions to previous data for natural specimens of zircon from Sri Lanka (Weber *et al.* 1994). Two additional specimens of intermediate-to-high α-decay dose from Sri Lanka also were examined. A similar comparison is made for the case of ion-irradiated synthetic thorite (tetragonal $ThSiO_4$) and natural thorite from the Kipawa complex, Villedieu Township, Quebec and from Brevig, Norway. The dose for amorphization is determined as a function of temperature for the ion-irradiated specimens, and the validity of comparing ion-irradiated synthetic specimens with α-decay-damaged minerals is evaluated. A recent model used to predict the crystalline-to-metamict transformation in natural zircon (Meldrum *et al.* 1998a) is further developed to include thorite and huttonite, and to delineate a range of radiation damage from barely detectable to complete amorphization, as measured by electron diffraction.

Crystal Structures

Zircon is made up of ZrO_8 polyhedra and SiO_4 tetrahedra (space group $I4_1/amd$, $Z = 4$; Fig. 1). These basic units alternate to form edge-sharing ZrO_8–SiO_4 chains parallel to the *c* axis (Hazen & Finger 1979). In metamict zircon, however, the Zr is only 7-fold coordinated, and the average Zr–Zr and Zr–O interatomic distances are lower (Farges & Calas 1991, Farges 1994).

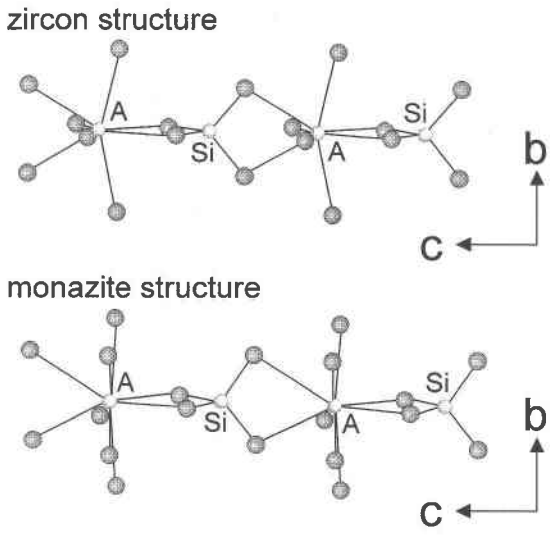

FIG. 1. Ball-and-stick crystal-structure diagrams of thorite and huttonite, modified from Taylor & Ewing (1978). Zircon and hafnon are isostructural with thorite. The two structures are closely related. In the higher-symmetry structure of thorite, the Th is coordinated to eight atoms of oxygen, but in the huttonite structure, the Th is 9-coordinated. In both structures, the thorium polyhedra share edges with SiO_4 tetrahedra to form chains parallel to the *c* axis.

Thorite in its crystalline form is isostructural with zircon, but metamict zircon and thorite do not share the same bonding geometry. The thorium sites in metamict thorite retain their original 8-fold geometry (Farges & Calas 1991). Hafnon also is isostructural with zircon, but there are no previous studies of the structure of amorphous or metamict hafnon.

Thorite is commonly metamict and hydrated [*e.g.*, as thorogummite $Th(SiO_4)_{1-x}(OH)_{4x}$: Frondel (1953)], and hydration may enhance the process of metamictization (Taylor & Ewing 1978). Thorite is less ubiquitous than zircon in crustal rocks, and its rare occurrence in sedimentary sequences suggests that it is less resistant than zircon to mechanical and chemical degradation during erosion and transport. The zircon–thorite phase diagram is not completely known, but a relatively wide miscibility gap has been proposed (Mumpton & Roy 1961, Speer 1982a) on the basis of the apparent absence of intermediate compositions in nature. In contrast, several lines of evidence suggest a complete solid-solution between the isostructural end-members zircon and hafnon (Speer 1982a).

Huttonite is the monoclinic polymorph of $ThSiO_4$ and has the monazite structure (space group $P2_1/n$; $Z = 4$; Taylor & Ewing 1978; Fig. 1). The thorium is coordinated to nine atoms of oxygen, and the SiO_4 tetrahedra are slightly distorted. These transformations lead to a more compact structure, and the density of huttonite is correspondingly higher (7.3 *versus* 6.7 g/cm^3 for pure huttonite and thorite, respectively). Reports of the natural occurrence of huttonite in the literature are relatively rare; however, where documented, huttonite appears to be invariably crystalline (Speer 1982b). This observation has previously led to the conclusion that huttonite is more "resistant" to radiation damage than thorite (Pabst 1952, Taylor & Ewing 1978). The thorite–huttonite phase diagram is unusual in that huttonite is the stable phase at both high temperature and high pressure (Dachille & Roy 1964).

EXPERIMENTAL

Zircon specimens from the well-studied Sri Lanka zircon gravels (*e.g.*, Holland & Gottfried 1955, Vance & Anderson 1972, Murakami *et al.* 1991, Woodhead *et al.* 1991, Weber *et al.* 1994) were provided by Prof. G.R. Rossman (sample numbers GRR 1468 and GRR 340). The crystals of natural thorite used in this investigation were obtained from two localities: 1) the Kipawa alkaline syenite pegmatites from Villedieu Township, Quebec (Currie & van Breemen 1994), and 2) nepheline syenites from Brevig, Norway. The crystals of Kipawa thorite are brick red, euhedral dipyramids approximately 2 cm across that contain visible inclusions of quartz. The Brevig thorite consists of dark brown fragments, the crystallographic orientation of which is difficult to ascertain. These latter specimens were first described by Pabst (1952) and found to be metamict.

The synthetic crystals of all four orthosilicate materials (zircon, hafnon, thorite, and huttonite) were grown by a high-temperature solution process employing a lithium molybdate flux. The resulting crystals are 2 to 10 mm in diameter, transparent and colorless. Several of the crystals were analyzed by X-ray diffraction to establish the appropriate structure-type, and their chemical composition was determined by energy-dispersion X-ray spectrometry (EDS) analysis in the TEM. For quantitative EDS measurements, the background was subtracted using the standard "window" method, and k-factors were predetermined from mineral standards.

Both the synthetic specimens and the natural Kipawa thorite were prepared for transmission electron microscopy (TEM) by hand polishing to a thickness of ~10 μm and then ion milling to perforation using 4 keV Ar^+ ions. The Brevig thorite consists of small, poorly formed grains that could not be mounted on a copper grid, so the specimens were prepared by crushing the grains in an agate mortar and transferring the resulting powder to a "holey" carbon-coated TEM grid.

The single-crystal TEM specimens were irradiated at the HVEM–Tandem facility at Argonne National Laboratory. This facility consists of a high-voltage Kratos/AEI transmission electron microscope interfaced to a Tandem ion accelerator, allowing for ion irradiations to be conducted *in situ* in the TEM. Irradia-

tions were performed with 800 keV Kr^+ ions. This relatively high energy was chosen so that most of the ions pass through the electron-transparent part of the specimen, thereby reducing the effects of implanted impurities. The flux was 1.7×10^{12} ions/cm^2/s. Selected-area electron diffraction and bright-field imaging techniques were used to monitor the transformation to the amorphous state. Thickness measurements were used to ensure that all diffraction measurements were taken from areas of the fringe with a constant thickness of ~100 nm. The samples are considered to be amorphous where the electron-diffraction pattern consists of only a diffuse diffraction halo. Care was taken to ensure that the electron beam did not remain on any given area of the specimen so as to avoid potential effects from prolonged electron irradiation. The experimental error was calculated by repeating the experiments three times at room temperature. The maximum difference between the highest and lowest measured fluence for amorphization, in units of ions/cm^2, was ~20%. The fluence for amorphization was monitored at temperatures ranging from –250 to 850°C. These temperatures were achieved using either a heating stage or a liquid-helium-cooled cooling stage. The accuracy of the thermocouple readings was previously estimated by monitoring the structural phase-transitions that occur in $SrTiO_3$ (–165°C), $BaTiO_3$ (120°C) and $KNbO_3$ (417°C). In all cases, the phase transitions were found to occur at temperatures within 15°C of the thermocouple reading.

The electron-diffraction criterion used in the present study to judge amorphous specimens has important limitations. For example, Miller & Ewing (1992) used image-simulation techniques to estimate the detection limits of electron diffraction for crystalline material embedded in an amorphous matrix, and *vice versa*. They found that up to 15% of crystalline material would not be detectable for a specimen thickness of 10 nm, although for thicker specimens the detection limit is lower. Salje *et al.* (1999) used diffuse X-ray scattering to determine that residual crystallinity may exist in samples previously thought to be metamict (Murakami *et al.* 1991). Hence, the electron-diffraction criterion is not meant to represent "complete" amorphization, but is used as a comparative tool to judge an essentially equivalent amorphous content (estimated at 95% for the present experiments). Furthermore, residual electron-diffraction maxima from crystalline material that may not be observable by eye may be visible in photographic negatives. In the present work, the amorphization dose was obtained by visual inspection of the electron-diffraction patterns on the TEM screen, and not by taking a series of negatives for each data point.

The amorphization fluence for 800 keV Kr^+ ions was converted to an equivalent displacement dose, D_c, in units of displacements per atom (dpa), using the Monte Carlo computer code Transport and Range of Ions in Matter (TRIM–96: Ziegler 1996). This allows for a direct comparison of damage in terms of the number of atomic displacements per atom (dpa) received by the material. A value of 0.5 dpa means that, on average, half of the atoms in the specimen have been displaced a single time. The fluence-to-dose conversion requires some knowledge of the energies associated with atomic displacements of the constituent atoms in the irradiated compounds. These values are unavailable for thorite, huttonite, and hafnon, so we used the values for zircon for all of the materials investigated (79, 23, and 47 eV for Zr, Si, and O, respectively).

Results

Microstructure

The sequence of microstructures that develop with increasing dose of radiation in the specimens of Sri Lanka zircon (Weber *et al.* 1994), with some exceptions, resembles that obtained in the present ion-beam experiments. The effect of irradiation, as a function of increasing accumulation of damage, is demonstrated by the electron-diffraction patterns in Figure 2A–D, which show a gradual decrease in intensity of the original diffraction-maxima with a concomitant increase in the intensity of the diffuse halo. In the present experiments, two additional samples of zircon from Sri Lanka of intermediate-to-high α-decay dose also were examined. Specimen GRR 1468 was found to be fully metamict. The specimen contains a total of ~0.75 wt.% $(U,Th)O_2$ as determined by EDS measurements, consistent with a previous chemical analysis of the same specimen (7600 ppm U; Woodhead *et al.* 1991). In contrast, specimen GRR 340 is composed of fine-grained, randomly oriented zircon "nanocrystals" (Fig. 3). The average grain-size is 10 nm, and the corresponding electron-diffraction pattern is consistent with the zircon structure. The maximum concentration of uranium estimated by EDS is ~0.63 wt.% UO_2, close to the detection limit for the EDS system.

Grains that macroscopically appear to be single crystals but are actually composed of randomly oriented "nanocrystals" have been reported in the literature (*e.g.*, Lumpkin & Chakoumakos 1988, Meldrum *et al.* 1998a). Holland & Gottfried (1955) interpreted their X-ray-diffraction results for the Sri Lanka zircon as indicating a polycrystalline stage at intermediate dose of radiation, but this was not observed by Murakami *et al.* (1991). A similar microstructure has been observed to develop during ion-beam irradiation of monazite at temperatures well above the critical amorphization temperature T_c (the temperature above which amorphization cannot be induced by the ion irradiations). A comparable effect (termed "polygonization") was documented to occur as a result of heavy-ion irradiation of a Pb–La–Zr–Ti (PLZT) oxide at a temperature of 450°C (Wang *et al.* 1993). This microstructure may, therefore, develop in

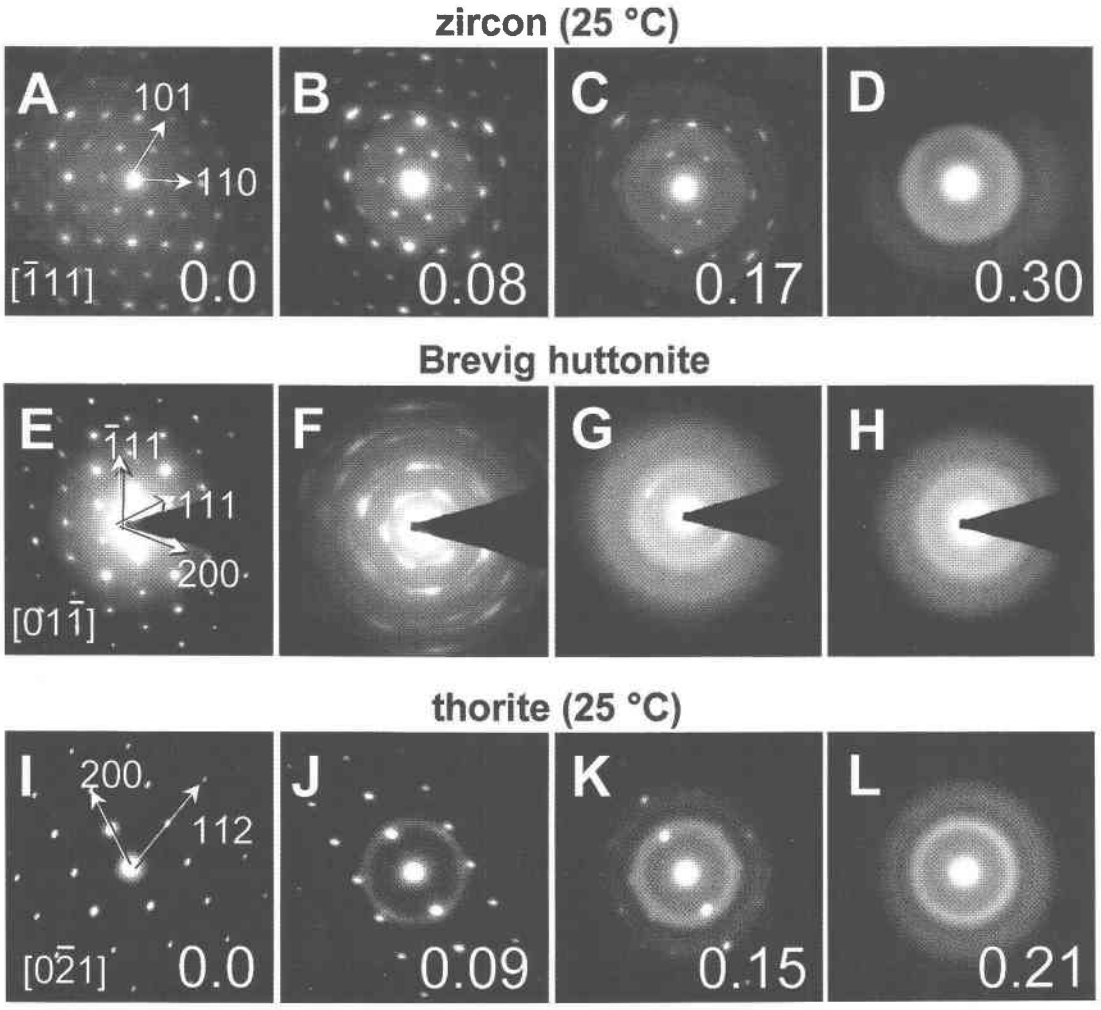

FIG. 2. Sequences of electron-diffraction patterns for zircon irradiated with 800 keV Kr^+ ions at room temperature (A–D), natural huttonite from Brevig, Norway (not irradiated: E–H) and ion-irradiated synthetic thorite (I–L). For the ion-beam-irradiated specimens of zircon and thorite, the corresponding dpa value is given in the bottom right of each diffraction pattern.

minerals as a result of α-recoil events during periods of elevated temperature.

TEM analysis of the Kipawa thorite showed minor inclusions of quartz and iron oxide. The quartz was readily distinguishable in bright-field images by its irregular morphology. Some of the included quartz is metamict, as determined by electron diffraction. The chief impurities in the thorite, in order of decreasing abundance, are iron, calcium, uranium, and manganese. The Kipawa thorite contains domains ranging from fully metamict to nearly completely crystalline, and in several specimens, a fine-grained (nanometer-scale) randomly oriented polycrystalline microstructure was observed. The individual grains are roughly spherical and vary from 10 to 50 nm in diameter.

Most of the Brevig thorite was found to be metamict, as judged by electron diffraction, but isolated grains retain some measurable crystalline component. A sequence of electron-diffraction patterns is shown in Figure 2E–H. These diffraction patterns for the crystalline material are, however, indexable as huttonite, and not as thorite. At least some of the Brevig "thorite" is, therefore, actually huttonite. In areas of moderate damage, the diffraction spots are streaks, and there is a faint diffuse halo, suggesting that the material may consist of both amorphous and textured crystalline material. The

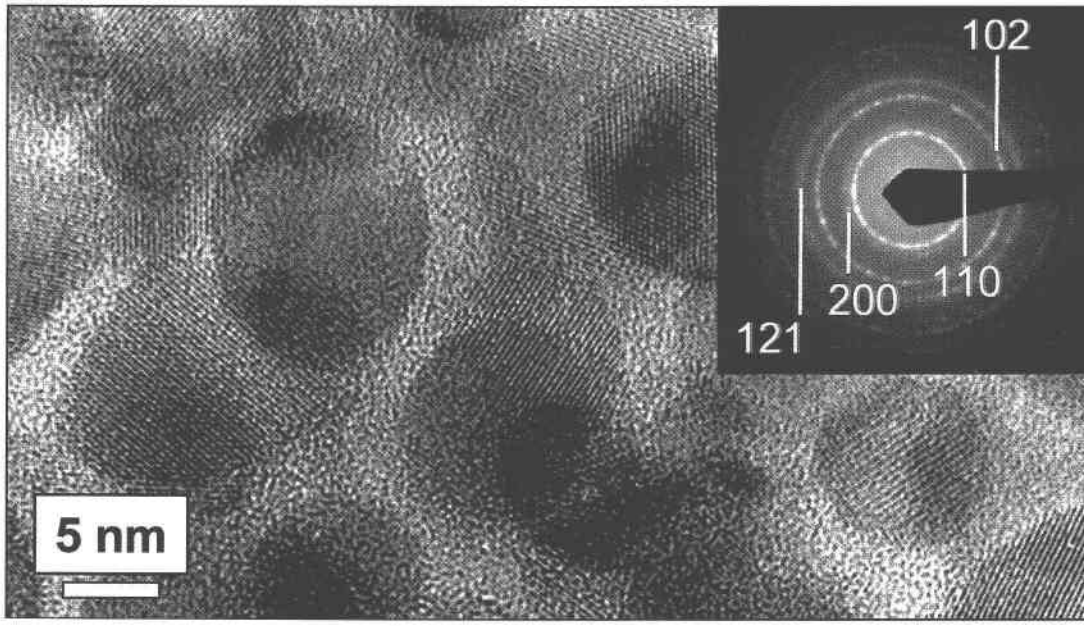

FIG. 3. High-resolution micrograph of zircon from Sri Lanka, sample GRR 340. The material is composed of randomly oriented polycrystalline zircon with an average grain-size of ~10 nm. The corresponding electron-diffraction pattern (inset) is unambiguously attributable to zircon.

diffraction streaks extend over approximately 20°, so the degree of grain orientation is lower than that for ion-beam-irradiated synthetic thorite and huttonite, which give relatively well-defined diffraction-maxima instead of streaks (Figs. 2I–L).

Previous spectrographic analysis of the Brevig thorite gave what were described as "large amounts" of Th and Si, "very small" amounts of Ca, Fe, and Mn, and "trace" concentrations of Li, Na, Mg, Al, B, Pb, and Ti (Pabst 1952). Li, B, and Na were not detected by EDS, as expected, but X-ray peaks from U were observed. Chemical variations between crystalline and metamict grains in the Brevig material are probably insufficient to account for the large differences in the degree of radiation damage, *i.e.*, from mostly crystalline to completely metamict. Grains of huttonite are known to recrystallize from metamict thorite upon heating above ~800°C (Pabst 1952, Robinson & Abbey 1957). The original thorite may, therefore, have contained grains of huttonite that did not become metamict or, alternatively, the huttonite may have formed by subsequent recrystallization.

Analysis of ion-beam-irradiated materials

The dose required for amorphization (D_c) is plotted as a function of temperature in Figure 4 for all the compounds investigated. The values obtained for D_c are a

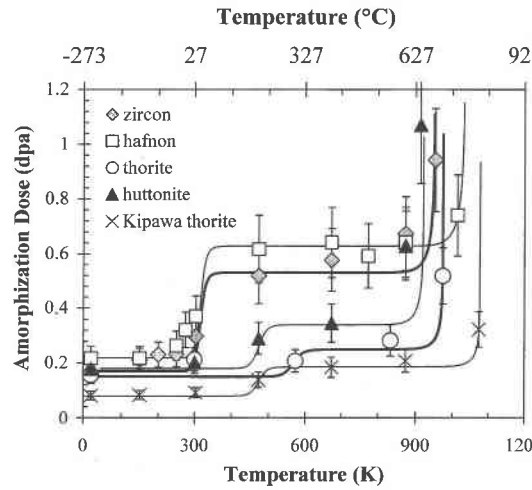

FIG. 4. Amorphization dose for 800 keV Kr^+ ions as a function of temperature for synthetic zircon, hafnon, thorite, huttonite, and natural thorite from Kipawa. The lines are plotted by "fitting" Equation 1 to the data (see text). The error bars were determined to be a maximum of ±20% by three repetitions of each room-temperature data point.

result of the competition between accumulation of radiation damage and simultaneous processes of thermal and irradiation-enhanced annealing. Hence, D_c is expected to be higher (*i.e.*, more annealing occurs) at higher temperatures of irradiation. For synthetic zircon and hafnon, the amorphization dose increases with temperature in two relatively well-defined "steps" (Fig. 4). These step-like increases are a result of annealing processes that are simultaneous with the ion irradiation. The first stage of annealing (Stage I) occurs over the temperature range of 10 to 80°C for zircon and hafnon. Stage II occurs at temperatures above 600°C. The data for huttonite suggest a similar Stage-I "step" between 25 and 200°C. In the cases of both the synthetic thorite and the natural Kipawa thorite, Stage-I annealing, if present, is more difficult to resolve. The natural thorite requires a lower dose for amorphization at all temperatures than did the synthetic material.

The lines plotted in Figure 4 are calculated from a recently developed amorphization–recrystallization model (Meldrum *et al.* 1999). According to this model, the irradiation time (t) to produce a given amorphous fraction (f_a) is related to the specimen temperature (T) through activation energies for Stage I [$E_{a(I)}$] and Stage II [$E_{a(II)}$] annealing:

$$f_a = \frac{P}{P+\lambda_I'}\cdot\left[1-e^{-(P+\lambda_I')\cdot\left[(1-\varepsilon)\cdot t+\frac{\varepsilon}{\lambda_{II}}\cdot(1-e^{-\lambda_{II}\cdot t})\right]}\right] \quad (1)$$

where P is the rate of disordering (in units of dpa/s), t is the duration of the irradiation time (in seconds), ε is the experimentally determined ratio of displacement damage that recovers by the Stage-I annealing process [$\varepsilon = (D_{0(II)}-D_{0(I)})/D_{0(II)}$], $\lambda_I' = A\exp(-E_{a(I)}/kT)/(1-\varepsilon)$, $\lambda_{II} = A\exp(-E_{a(II)}/kT)$, k = Boltzmann's constant, A is the lattice-vibration frequency (~10^{13} Hz), and D_0 is the amorphization dose extrapolated to –273°C (Table 1). For the purpose of these calculations, the amorphous fraction required to produce a diffuse halo in the electron-diffraction pattern is assumed to be 95%, an estimate based on the image-simulation results of Miller & Ewing (1992).

In Equation 1, the activation energy $E_{a(I)}$ determines the temperature range for the "step" increase at intermediate temperatures, ε gives the "height" of the step, and $E_{a(II)}$ determines the temperature dependence of the amorphization dose at high temperature. These parameters are all "fit" to the data to minimize the difference between the experimental data-points and the calculated values. The fit was determined by the standard linear least-squares method. In cases where there is a large gap in the data in the temperature range for Stage-I annealing (*e.g.*, synthetic thorite), then the true activation energy could be anywhere between the bracketing data-points. For all compounds, the best fit is obtained by assuming two-stage behavior. In general, the best fit to the data obtained with Equation 1 is less satisfactory than that obtained by using semi-empirical models relating the amorphization dose to temperature (*e.g.*, Weber *et al.* 1994); however, the previous models generate unrealistic activation energies for proposed physical processes (*e.g.*, values as low as 0.005 eV have been obtained; Devanathan *et al.* 1998) and contain other factors of undefined physical meaning (theoretical arguments to this effect have been published elsewhere: Meldrum *et al.* 1999).

The activation energies for Stage-I annealing in the orthosilicates were estimated to be ~1.0 eV. Since the errors in these values are nearly entirely dependent on the number of data points in the Stage-I temperature range, a range of possible activation energies is given in Table 2. The activation energy increases from 3.1 to 3.7 eV for the Stage-II annealing process (Table 2). These values were obtained by constraining the curves to pass

TABLE 1. EXPLANATION OF SYMBOLS

Symbol	Units	Comments
ε	none	experimentally determined ratio of D_0 values for Stage-I and Stage-II annealing
λ	seconds^{-1}	rate constant for annealing process
A	seconds^{-1}	atomic vibration frequency (10^{13} Hz)
C	none	constant in Equations 4-8
D_c	dpa	dose for amorphization
$D_{0(I)}$	dpa	extrapolated dose for amorphization at 0 K (Stage I)
$D_{0(II)}$	dpa	extrapolated dose for amorphization at 0 K (Stage II)
$E_{a(I)}$	eV	activation energy for Stage-I annealing
$E_{a(II)}$	eV	activation energy for Stage-II annealing
f_a	none	amorphous fraction
k	eV•K^{-1}	Boltzmann's constant (= 0.000086 eV•K^{-1})
Nc	ppm	critical radionuclide concentration for metamictization
P	dpa/s	damage rate
T_c	°C	critical temperature above which amorphization does not occur
t	seconds	irradiation time
X	none	constant in Equations 4-8

TABLE 2. EXPERIMENTAL PARAMETERS USED IN EQUATION 1

Compound	$E_{a(I)}$ (eV)	$E_{a(II)}$ (eV)	ε	$D_{0(I)}$	$D_{0(II)}$
Zircon	1.0 ± 0.1[1]	3.3[2]	0.68	0.17	0.50
Hafnon	1.0 ± 0.1	3.6	0.65	0.22	0.62
Huttonite	1.2 ± 0.3	3.1	0.47	0.18	0.34
Thorite	1.0 ± 0.9	3.3	0.40	0.15	0.25
Kipawa thorite	1.3 ± 0.3	3.7	0.57	0.08	0.18

[1] The error in $E_{a(I)}$ is based on the range of possible values that would give equally good fits to the data.
[2] No error is given because the curves were constrained to pass through the highest-temperature data-point.

through the highest temperature data-point for each phase. These activation energies for Stage-I and Stage-II annealing can be compared to the known activation energies for various processes of defect migration. Stage-I values are quite close to energies of interstitial migration for insulating ceramics such as MgO and Al_2O_3 (Zinkle & Kinoshita 1997). The activation energy obtained for Stage-II annealing in zircon (3.3 eV) is slightly lower than the value of 3.6 eV recently obtained for annealing of fission tracks parallel to the *c* axis in zircon (Virk 1995). The process responsible for Stage-II annealing may, therefore, be irradiation-enhanced epitactic recrystallization of bulk amorphous zones.

An expression for T_c, the critical temperature above which amorphization will not occur, was previously obtained (Meldrum *et al.* 1999):

$$T_C = \frac{E_a}{k \cdot \ln\left[\frac{A \cdot f_a}{P(1-\varepsilon)\cdot(1-f_a)}\right]} \quad (2)$$

T_c is the temperature above which the annealing processes are faster than those of damage accumulation. The critical temperatures calculated using Equation 2 for the orthosilicates are given in Table 3. The values obtained for T_c are linearly related to $E_{a(II)}$ and are, therefore, most accurate for cases where data-points for high-dose samples exist. The amorphization dose for the orthosilicates is relatively low even at the highest obtainable temperatures, so the calculated values of T_c are probably slightly low.

A further effect occurs during irradiation at elevated temperatures. Above 600°C, zircon first becomes amorphous, but with increasing dose, it gradually decomposes into nanocrystalline cubic or tetragonal ZrO_2 and amorphous SiO_2 (the distinction between the cubic and tetragonal phases of ZrO_2 could not be conclusively determined by electron diffraction). At temperatures above 750°C, the single-crystal zircon decomposed directly into the component oxides without an intermediate amorphous phase. The resulting microstructure consisted of randomly oriented nanometer-scale grains of ZrO_2 in a matrix of amorphous SiO_2 (Fig. 5). The

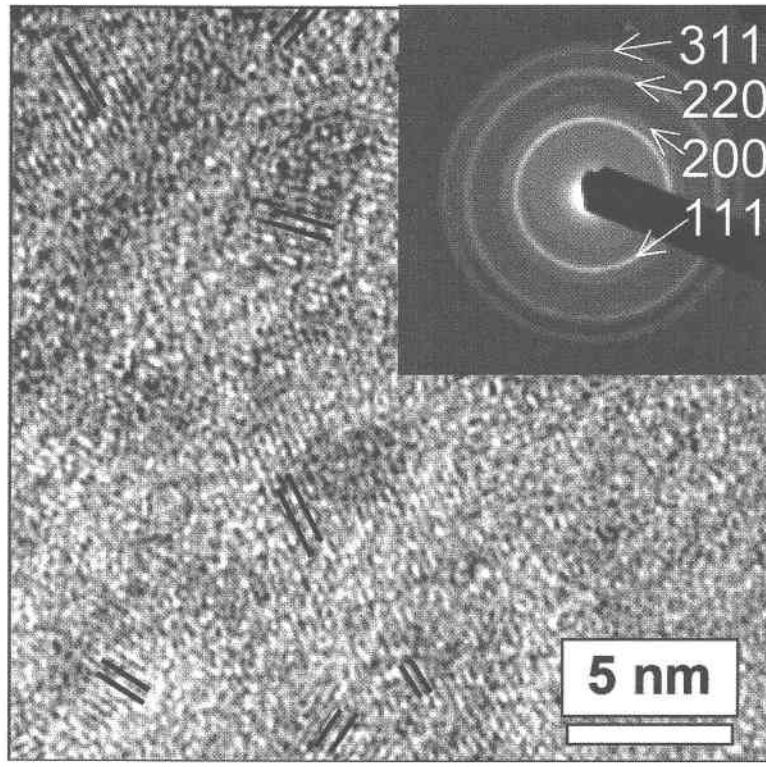

FIG. 5. High-resolution TEM micrograph showing randomly oriented nanocrystalline grains of cubic or tetragonal ZrO_2 embedded in amorphous silica. The specimen was irradiated at 800°C to a dose of 3 dpa. The orientation of the lattice fringes is highlighted by the dark lines.

TABLE 3. CONSTANTS USED IN EQUATIONS 4–8

Compound	T_c (°C)[1]	T_c (°C)[2]	C[3]	X
Zircon (I)[4]	25	–110	0.66	170
Zircon	700	250	14.5	470
Huttonite	650	220	3.4	302
Thorite	700	260	4.2	232
Kipawa thorite	800	310	3.4	190

[1] Critical temperature calculated for a dose rate of 0.002 dpa/s (equivalent to ion-beam experiments).
[2] Critical temperature calculated for a dose rate of 5×10^{-18} dpa/s (equivalent to geological specimens).
[3] C is a constant obtained from the model of Weber *et al.* (1994).
[4] Stage-I data are presented only for zircon. All other data refer to Stage-II annealing.

temperatures required to form the component oxides during irradiation were higher by approximately 50 and 150°C in hafnon and thorite, respectively. In the case of huttonite, epitactic recrystallization at elevated temperatures restricted the formation of the component oxides. The cubic and tetragonal phases of the metal oxide are metastable at room temperature and could, over time, revert to the stable monoclinic form (*i.e.*, as baddeleyite). This process could, in part, account for the reported occurrence of particles of monoclinic ZrO_2 in metamict zircon (*e.g.*, Vance & Anderson 1972, Vance 1974). The physical process responsible for the phase decomposition was investigated in detail and reported elsewhere (Meldrum *et al.* 1998b).

At temperatures above 700°C, huttonite recrystallizes epitactically from the thick portions of the TEM foil not penetrated by the ion beam. In comparison, zircon, hafnon, and thorite did not recrystallize at the maximum obtainable temperatures in the TEM (850°C). Huttonite and thorite require a similar ion-dose to become amorphous over a wide range of temperatures (Fig. 4). Thus, huttonite is not "more resistant" to radiation damage, but is more easily recrystallized by purely thermal processes.

Discussion

Several important similarities and differences exist among ion-irradiated specimens and minerals that undergo radiation damage from α-decay processes. In most cases, the sequence of microstructures that occur with increasing dose of radiation are similar. The materials pass through four arbitrarily defined stages (Murakami *et al.* 1991): Stage 1: Dose = 0: completely crystalline. Stage 2: Dose ≈ $0.3D_c$: isolated amorphous domains enclosed by undamaged, crystalline material. Stage 3: Dose ≈ $0.7D_c$: isolated crystalline "islands" embedded in an amorphous matrix. Crystallites may be rotated by ±5° from the original orientation owing to strain effects (Weber *et al.* 1994). Stage 4: Dose = D_c: the material is amorphous, as measured by electron diffraction and phase-contrast imaging techniques.

In the natural specimens, however, a fine-grained polycrystalline texture may be observed in some specimens of intermediate α-decay dose that has not been reproduced in ion-irradiation experiments except at temperatures well above T_c. The formation of this microstructure could, therefore, occur as a result of α-decay processes that occurred during periods of elevated temperature. Alternatively, alteration of the metamict phase may occur at elevated pressure and temperature in the presence of fluids. A more detailed analysis is planned for future work.

In the high-dose-rate regime of the ion-beam-irradiated materials (P = 0.002 dpa/s), the calculated T_c for zircon is approximately 700°C. The dose rate in natural zircon is lower by approximately 14 orders of magnitude, as compared with the ion-beam experiments. Zircon (or other minerals) may gradually recover by thermal diffusion processes that occur over millions of years. Thus the effective critical temperature is expected to be lower in natural samples. In the case of zircon, inserting a damage rate of 5.2×10^{-18} dpa/s into Equation 2 (equivalent to a zircon crystal with 1000 ppm U) gives a T_c of ~250°C (Fig. 6). At temperatures above 250°C, annealing of α-recoil tracks is faster than the accumulation of damage.

The dose rate for natural specimens, however, is not actually constant; it decreases slowly with time as the radioactive isotopes decay. Nonetheless, this point has only a minor effect on the calculated value of T_c. For example, a zircon grain with initially 1000 ppm equivalent uranium (eU) will have an initial dose-rate of 5.2×10^{-18} dpa/s. After 500 Ma, the uranium concentration will be 925 ppm, and the dose rate will have decreased

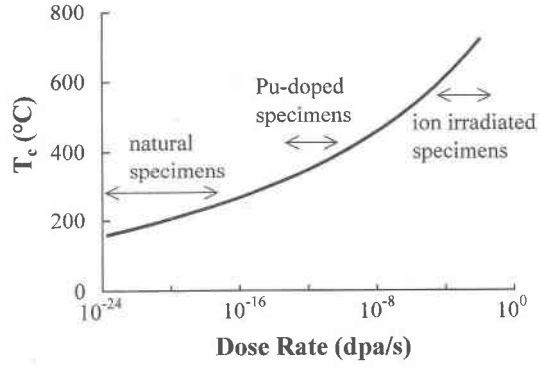

FIG. 6. Dose-rate dependence of the critical temperature calculated from Equation 2. Typical ranges of dose-rate values for grains of natural zircon, Pu-doped zircon, and for ion-irradiated zircon are indicated.

to 4.8×10^{-18} dpa/s. The corresponding decrease in T_c is only 0.5°C and can, therefore, be ignored in these calculations. For most natural specimens of zircon, T_c is essentially constant at ~250°C.

Previously, Meldrum *et al.* (1998a) derived the following general expression relating the *present-day* concentration of equivalent uranium for metamictization, N_c, to the age, t, of a given mineral grain as a function of temperature T:

$$N_c(ppm) = \left[\frac{X}{\left[1 - e^{C\cdot(1-T_c/T)}\right] \cdot (e^{\lambda\cdot t} - 1) \cdot n \cdot x} \right] \quad (3)$$

where C is an experimentally determined constant (Weber *et al.* 1994, Meldrum *et al.* 1998a), $X = [6 \bullet 10^6 \bullet D_0]$, n is the average number of atomic displacements per α-decay, and x is the number of α-decays in the decay chain. Equation 3 is based on a previous semi-empirical model used to obtain the temperature dependence of the amorphization dose (Weber *et al.* 1994), and not on Equation 1. Equation 1 could, in principle, be used to derive the critical concentration of uranium for zircon (and the other orthosilicates) by solving for D_c at the temperature of interest, obtaining the dose-rate dependence of T_c (Eq. 2), and calculating the uranium concentration necessary to produce D_c in time t (corresponding to the age of the sample) for this new value of T_c. However, the physical reality of the model used to calculate D_c is irrelevant for the calculation of N_c; all that is required is that the model accurately fits the data. Since a previous semi-empirical model does give the best fit, Equation 3 remains valid.

Equation 2 has some important implications for the calculation of N_c. We previously suggested that Stage-I data had to be used for temperatures below 200°C for zircon (Meldrum *et al.* 1998a). Equation 2 can, however, be used to calculate an *effective* value of T_c for the Stage-I process also. In other words, in the low-dose-rate regime of the natural specimens, Stage-I annealing may occur at lower temperatures than in the ion-beam experiments, which is identical to the above analysis for the Stage-II process. By inserting the activation energy for Stage-I annealing in zircon (1 eV) into Equation 2 and using $P = 5 \times 10^{-18}$ dpa/s, the low-temperature annealing should be complete at temperatures above –110°C (Table 3). Since such low temperatures do not occur in the geological environment, the Stage-I annealing is completed in the natural specimens, and one need only model the Stage-II process. Thus, Stage-II data for Equation 3 with $T_c = 260$°C should ideally be used without low-temperature modifications. Equation 3 then can be solved for the specific case of zircon:

$$N_c(ppm) = \frac{470}{\left[1 - e^{14.5\cdot(1-523/T)}\right] \cdot (e^{1.55\cdot10^{-10}\cdot t} - 1)} \quad (4)$$

According to Equation 4, for present-day concentrations of equivalent uranium above N_c in zircon of age t (expressed in years) at temperature T, the grain should be metamict. Thus if a temperature of 100°C is assumed for the Sri Lanka specimens of zircon, which have an age of 570 Ma, then N_c is 5100 ppm eU. Grains with a higher concentration of equivalent uranium should be metamict. This value of N_c is higher than that calculated previously (Meldrum *et al.* 1998a). Since the X-ray-diffraction results of Murakami *et al.* (1991) indicate a critical concentration of uranium of ~3300 ppm eU, the values calculated from Equation 4 are high. The high values are caused by the selection of $D_0 = 0.5$ dpa for the Stage-II process, leading to a high value for X in Equation 3. The value of 0.5 dpa is higher than the D_c for Pu-doped zircon (Weber 1990) and for the Sri Lankan zircon (Murakami *et al.* 1991, Weber *et al.* 1994), which strongly suggests that D_0 for Stage II is indeed too high. If the experimentally determined value of D_0 for Stage-I is used instead, then Equation 4 can be rewritten:

$$N_c(ppm) = \frac{170}{\left[1 - e^{0.66\cdot(1-523/T)}\right] \cdot (e^{1.55\cdot10^{-10}\cdot t} - 1)} \quad (5)$$

This is similar to Equation 12 in Meldrum *et al.* (1998a) and gives similarly good results when compared to the experimental data for the specimens of Sri Lankan zircon studied by Murakami *et al.* (1991). At this point, it is not understood why D_0 for Stage I gives better results. Possible explanations include: i) an overestimate of D_0 for the Stage-II process due to a lack of sufficient data-points in Figure 4 and the relatively large experimental error, or ii) the large surfaces in the thin TEM samples may act as a sink for defects during irradiation, resulting in a higher amorphization dose. In the worst case, the assignment of two separate annealing stages is in error, despite the better model fit to the data. In any case, Equation 5 is recommended for calculations of N_c in zircon.

Thus far, the crystalline-to-metamict transformation has been modeled as a sharp transition; in other words, we have not plotted a transition zone, but have simply assumed that a grain of zircon containing an equivalent uranium concentration above N_c will be "metamict", and below N_c it will be "crystalline". This is clearly a simplification of the actual situation. For example, Lumpkin & Ewing (1988) were able to clearly determine the range of α-decay doses in pyrochlore required to produce "barely detectable" damage to "complete" amorphization. The calculation of N_c gives the upper boundary for metamictization, subject to the constraints of the electron-diffraction technique. A lower boundary can also be estimated from the present data. According to Miller & Ewing (1992), the minimum amount of amorphous material required to be detectable by electron dif-

fraction is approximately 35%. If we assume a direct-impact model for the amorphization of zircon, as opposed to a multiple overlap of collision cascades, then the following equation relates the amorphous fraction, f_a, to the amorphization dose (Weber *et al.* 1990):

$$f_a = 1 - \exp(-BD_c) \quad (6)$$

where B is a constant. According to Equation 6, if f_a is decreased from 95% to 35%, then D_c decreases by a factor of 0.85. A value of $0.15D_c$ can, therefore, be used to estimate the minimum detectable fraction of radiation damage required to be detectable in the TEM. Since N_c is linearly related to D_0 (Eq. 3), the minimum detectable amorphous fraction occurs at a value of $0.15N_c$.

Figure 7 shows a plot of N_c as a function of age for zircon at a temperature of 100°C. A transition zone also is plotted; it brackets a range of amorphous fractions from $f_a = 0.35$ to 0.95. The values of N_c obtained from both Equation 4 (thin lines) and 5 (thick lines) are shown. Selected grains of crystalline and metamict zircon from the literature are plotted for comparison to the model. The age of the metamict grains was obtained by dating cogenetic crystalline samples. In some cases, the thorium concentration was not given, and the eU values are probably slightly low. The crystalline–metamict boundaries are shifted somewhat compared to our earlier model (Meldrum *et al.* 1998a) owing to these new calculations for T_c. The calculated values of N_c at 25°C delineate the boundary between crystalline and

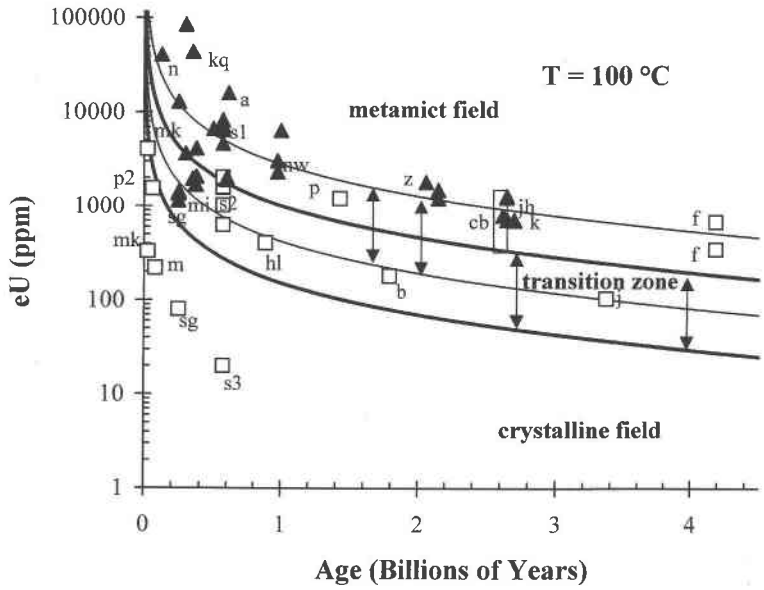

FIG. 7. The transition zone from the crystalline state to the metamict state as a function of age and concentration of equivalent uranium (eU) for zircon at 100°C. The transition zone delineates the boundary between crystalline and metamict zircon. The thick lines are for $D_0 = 0.17$ (Stage I), and the thinner lines are for $D_0 = 0.50$ (Stage II). Data for selected specimens of crystalline and metamict zircon are also plotted for comparison. Data and localities as follows: a: Ampangabe, Malagasy Republic (Farges & Calas 1991), b: Bonner Formation, Montana (Parrish 1990), cb: range of values for the Cartier Batholith, Ontario (Meldrum *et al.* 1997b), f: Mt. Narryer, Australia (Froude *et al.* 1983; highest and lowest values only), hl: Himalaya leucogranite (Zeitler & Chamberlain 1991), jh: Jack Hills, Australia (Heaman & Parrish 1991), k: Kartashovo region, central Karelia (Makayev *et al.* 1981), kq: Kinkle's Quarry, N.Y. (Farges & Calas 1991), m: Mojave, California (Silver 1991), mi: Miask, Russia (Farges & Calas 1991), mk: Mae Klang granite, Thailand (Dunning *et al.* 1995), n: Naegy, Japan (Farges & Calas 1991), nw: Norway (Deliens *et al.* 1977), p: Passmore, British Columbia (Parrish 1990), s1 and s2: Sri Lanka (Woodhead *et al.* 1991), sg: Saxonian granulite, Germany (Nasdala *et al.* 1996), z: "highly metamict" zircon from lower Democratic Republic of Congo (Deliens *et al.* 1977). The unlabeled points represent samples of metamict zircon from various localities, described by Kulp *et al.* (1952), and recalculated to equivalent U-concentration from the given activity values.

metamict zircon from the literature, suggesting that the above analysis is essentially correct. With the exception of the 4.2 Ga zircon from Mt. Narryer, Australia (Froude *et al.* 1981), none of the selected data from the literature plot in the wrong field. Both crystalline and metamict grains of zircon plot in the transition zone. The Mt. Narryer data imply that at least some of the 4.2 Ga zircon grains experienced significantly higher temperatures.

Using a similar derivation as that given in Meldrum *et al.* (1998a) for zircon, the N_c values for pure thorite and huttonite also can be calculated:

$$\text{thorite: } N_c(ppm) = \frac{232}{\left[1-e^{4.2(1-523/T)}\right]\cdot\left(e^{4.95\cdot10^{-11}\cdot t}-1\right)} \quad (7)$$

$$\text{huttonite: } N_c(ppm) = \frac{302}{\left[1-e^{3.4(1-494/T)}\right]\cdot\left(e^{4.95\cdot10^{-11}\cdot t}-1\right)} \quad (8)$$

where, in this case, the N_c values are obtained in units of equivalent thorium. The constants in the numerator and in the left-hand exponent term in the denominator (Table 3) were obtained exactly as described in Meldrum *et al.* (1998a) for zircon. For zircon and huttonite, the potential problems arising from the interpretation of two stages of annealing are minimal because the difference in D_0 between Stage I and Stage II is small.

The time required for thorite and huttonite to become metamict owing to self-radiation damage is plotted as a function of ambient temperature in Figure 8. For a temperature of 100°C, pure thorite actually becomes metamict owing to self-radiation damage after 5 Ma. If thorite grains older than 5 Ma are found to be crystalline, then they probably experienced higher temperatures; these temperatures can, in fact, be estimated from Equation 7. On the basis of the results in Figure 8, we predict that huttonite would require a longer time to become metamict than thorite under identical ambient conditions. At 100°C, pure huttonite should become metamict owing to self-radiation damage after 7 Ma (Fig. 8). The difference between thorite and huttonite is enhanced at higher temperatures. For example, at 220°C (close to T_c for huttonite), pure thorite requires 15 Ma to become metamict, whereas chemically pure huttonite requires ~1000 Ma for the crystalline-to-metamict transformation to occur.

The impurities in the thorite may also play a role in the kinetics of amorphization. Lumpkin & Chakoumakos (1988) found that the presence of a phosphorus-bearing impurity in thorite could enhance the kinetics of recrystallization, whereas Meldrum *et al.* (1997a) found that monazite containing Th, Ca, Fe, and Si impurities could be amorphized at higher temperatures than pure $NdPO_4$. The consistently lower dose obtained in the ion-beam experiments for the Kipawa thorite, as compared with synthetic $ThSiO_4$ (Fig. 4), could be caused by impurities or by the presence of up to 35% metamict material already in the specimen prior to irradiation. However, radiation damage should not affect the annealing kinetics, and hence T_c should remain unchanged. T_c for the Kipawa thorite is, however, approximately 60°C higher than for pure $ThSiO_4$. This experimental result cannot be caused by the presence of previously existing radiation-induced damage. This difference in T_c is reflected in Figure 8, which shows that the Kipawa thorite would become metamict in a shorter time at any given temperature. The Kipawa thorite contains a variable but relatively large proportion of Fe, Ca, U, and Mn impurities, and these impurities may, therefore, impede the annealing process.

Limitations of analysis

Several important limitations exist in the preceding analysis. For example, the potentially important effects of impurities in zircon were not modeled. The differences shown in Figure 4 between $ZrSiO_4$ and $HfSiO_4$ suggest that the presence of Hf substituting for Zr could affect the actual value of N_c. The amorphization behavior has also been assumed to be the same for ion-irradiated thin films and α-decay-damaged minerals. A relatively large experimental error exists in the irradiation experiments, and errors may also arise in the application of Equation 1 with the assumption of two stages of annealing during irradiation. Despite these limitations, the data for zircon agree relatively well with the available data for both crystalline and metamict samples.

Conclusions

Radiation-damage effects in naturally irradiated zircon and thorite were compared with those observed in ion-beam-irradiated (800 keV Kr^+) synthetic specimens

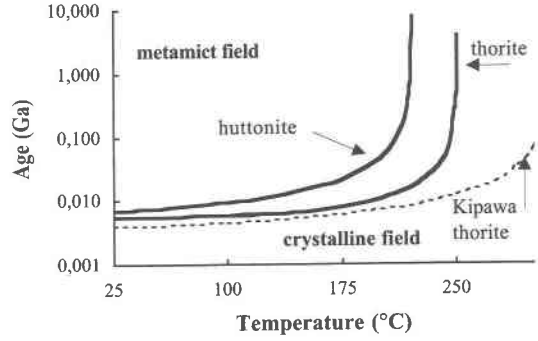

FIG. 8. Age and temperature dependence of the crystalline-to-metamict transformation in thorite and huttonite. For each curve, specimens in the upper field should be metamict, and those in the lower field, crystalline.

of zircon, hafnon, thorite, huttonite, and crystalline thorite from Kipawa. The amorphization dose was obtained as a function of temperature for the ion-irradiated samples. All of the specimens become amorphous at less than 1 dpa at temperatures below 600°C. At higher temperatures, the amorphization dose increases in the order: Kipawa thorite, synthetic thorite, hafnon, zircon, huttonite. Two stages of amorphization–annealing were identified, with activation energies of ~1.0 eV (Stage I) and 3.1 to 3.7 eV (Stage II).

Whereas natural zircon and thorite undergo radiation-induced amorphization that is generally similar to that produced by ion bombardment, the amorphization dose is significantly higher owing to long-term annealing effects. A previous model was further developed and applied to calculate the crystalline-to-metamict transformation in natural zircon, thorite, and huttonite. A comparison with literature data for known specimens of zircon demonstrates that the modeled results are reasonably accurate. Thorite is predicted to become metamict owing to self-radiation damage after relatively short times, whereas huttonite recovers more rapidly from the effects of irradiation and takes correspondingly longer to become metamict.

Acknowledgements

The authors thank the staff at the HVEM–Tandem Facility for assistance with the ion irradiations. This manuscript was greatly improved as a result of reviews by Drs. R.F. Martin, L. Galoisy, and an anonymous referee. Dr. W.J. Weber is thanked for several interesting and useful discussions on the interpretation of the amorphization data for zircon. We acknowledge the use of the SHaRE Facility in the Metals and Ceramics Division at ORNL. The specimens of Sri Lankan zircon were generously provided by Dr. George Rossman at Cal Tech. The Natural Sciences and Engineering Research Council of Canada has supported this research through a postdoctoral fellowship to A.M. S.J.Z acknowledges support from the Office of Fusion Energy Sciences, and R.C.E., from BES/DOE (DE–FG02–97ER45656). This work was supported by the U.S. Department of Energy, Division of Materials Sciences and Environmental Management Research Program (LAB). Oak Ridge National Laboratory is managed by Lockheed Martin Energy Research Corp. for the U.S. Department of Energy under contract number DE–AC05–96OR22464.

References

Berzelius, J. (1815): Undersökning af gadolinitens sammansättning. *Afhandl. Fys. Kem. Mineral.* **4**, 217-236.

Brøgger, W.C. (1890): Die Mineralien der Syenitpegmatitgänge der südnorwegischen Augit- und Nephelinsyenite. *Z. Kristallogr.* **16**, 1-658.

Currie, K.L. & van Breemen, O. (1994): Tectonics and age of the Kipawa syenite complex, western Quebec. *Geol. Assoc. Can. – Mineral. Assoc. Can., Program Abstr.* **19**, A25.

Dachille, F. & Roy, R. (1964): Effectiveness of shearing stresses in accelerating solid phase reactions at low temperatures and high pressures. *J. Geol.* **72**, 243-247.

Deliens, M., Delhal, J. & Tarte, P. (1977): Metamictization and U–Pb systematics – a study by infrared absorption spectrometry of Precambrian zircons. *Earth Planet. Sci. Lett.* **33**, 331-344.

Devanathan, R., Weber, W.J., Sickafus, K.E., Nastasi, M, Wang, Lu-Min &Wang, Shi-Xin (1998): Cryogenic radiation response of sapphire. *Nucl. Instrum. Methods Phys. Res.* **B141**, 366-371.

Dunning, G.R., MacDonald, A.S. & Barr, S.M. (1995): Zircon and monazite U–Pb dating of the Doi Inthanon core complex, northern Thailand; implications for extension within the Indonesian Orogen. *Tectonophys.* **251**, 197-213.

Ewing, R.C. (1993): The metamict state: 1993 – the centennial. *Nucl. Instrum. Methods Phys. Res.* **B91**, 22-29.

Farges, F. (1994): The structure of metamict zircon: a temperature-dependent EXAFS study: *Phys. Chem. Minerals* **20**, 504-514.

_____ & Calas, G. (1991): Structural analysis of radiation damage in zircon and thorite: an X- ray absorption spectroscopic study. *Am. Mineral.* **76**, 60-73.

Frondel, C. (1953): Hydroxyl substitution in thorite and zircon. *Am. Mineral.* **38**, 1007-1018.

Froude, D.O., Ireland, T.R., Kinney, P.D., Williams, I.S., Compston, W., Williams, I.R. & Myers, J.S. (1983): Ion microprobe identification of 4,100 – 4,200 Myr.-old terrestrial zircons. *Nature* **304**, 616-618.

Hazen, R.M. & Finger, L.W. (1979): Crystal structure and compressibility of zircon at high pressure. *Am. Mineral.* **64**, 196-201.

Heaman, J. & Parrish, R.R. (1991): U–Pb geochronology of accessory minerals. *In* Applications of Radiogenic Isotope Systems to Problems in Geology (L. Heaman & J.N. Ludden, eds.). *Mineral. Assoc. Can., Short-Course Vol.* **19**, 59-102.

Holland, H. & Gottfried, D. (1955): The effect of nuclear radiation on the structure of zircon. *Acta Crystallogr.* **8**, 291-300.

Krogh, T.E. (1982): Improved accuracy of U–Pb zircon ages by the creation of more concordant systems using an air abrasion technique. *Geochim. Cosmochim. Acta* **46**, 637-649.

_____ & Davis, G.L. (1975): Alteration in zircons and differential dissolution of altered and metamict zircon. *Carnegie Inst. Wash., Yearbook* **74**, 619-623.

KULP, J.L., VOLCHOK, H.L. & HOLLAND, H.D. (1952): Age from metamict minerals. *Am. Mineral.* **37**, 709-718.

LUMPKIN, G.R. & CHAKOUMAKOS, B.C. (1988): Chemistry and radiation effects of thorite-group minerals from the Harding pegmatite, Taos County, New Mexico. *Am. Mineral.* **73**, 1405-1419.

_____ & EWING, R.C. (1988): Alpha-decay damage in minerals of the pyrochlore group. *Phys. Chem. Minerals* **16**, 2-20.

_____, HART, K.P., MCGLINN, P.J., PAYNE, T.E., GIERÉ, R. & WILLIAMS, C.T. (1994): Retention of actinides in natural pyrochlores and zirconolites. *Radiochim. Acta* **66/67**, 469-474.

_____, SMITH, K.L., BLACKFORD, M.G., GIERÉ, R. & WILLIAMS, C.T. (1998): The crystalline–amorphous transformation in natural zirconolite: evidence for long-term annealing. *Mater. Res. Soc., Symp. Proc.* **506**, 215-222.

MAKAYEV, A.I., LEVCHENKOV, O.A. & BUBNOVA, R.S. (1981): Radiation damage as an age measure for natural zircons. *Geokhimiya* **2**, 175-182 (in Russ.).

MELDRUM, A., ABDEL-RAHMAN, A., MARTIN, R.F. & WODICKA, N. (1997b): The nature, age, and petrogenesis of the Cartier Batholith, northern flank of the Sudbury Structure, Ontario, Canada. *Precamb. Res.* **82**, 265-285.

_____, BOATNER, L.A. & EWING, R.C. (1997a): Displacive radiation effects in the monazite- and zircon-structure orthophosphates (La–LuPO$_4$). *Phys. Rev. B* **56**, 13805-13814.

_____, _____, WEBER, W.J. & EWING, R.C. (1998a): Radiation effects in zircon and monazite. *Geochim. Cosmochim. Acta* **62**, 2509-2520.

_____, ZINKLE, S.J., BOATNER, L.A. & EWING, R.C. (1998b): A transient liquid-like state in the displacement cascades of zircon, hafnon, and thorite. *Nature* **395**, 56-58.

_____, _____, _____ & _____ (1999): Heavy-ion irradiation effects in the ABO$_4$ orthosilicates: decomposition, amorphization, and recrystallization. *Phys. Rev. B* **59**, 3981-3992.

MILLER, M.L. & EWING, R.C. (1992): Image simulation of partially amorphous materials. *Ultramicroscopy* **48**, 203-237.

MUMPTON, F.A. & ROY, R. (1961): Hydrothermal stability studies of the zircon–thorite group. *Geochim. Cosmochim. Acta* **21**, 217-238.

MURAKAMI, T., CHAKOUMAKOS, B.C., EWING, R.C., LUMPKIN, G.R. & WEBER, W.J. (1991): Alpha-decay event damage in zircon. *Am. Mineral.* **76**, 1510-1532.

NASDALA, L., PIDGEON, R.T. & WOLF, D. (1996): Heterogeneous metamictization of zircon on a microscale. *Geochim. Cosmochim. Acta* **60**, 1091-1097.

PABST, A. (1952): The metamict state. *Am. Mineral.* **37**, 137-157.

PARRISH, R.R. (1990): U–Pb dating of monazite and its application to geological problems. *Can. J. Earth Sci.* **27**, 1431-1450.

ROBINSON, S.C. & ABBEY, S. (1957): Uranothorite from eastern Ontario. 1. Occurrence and description. *Can. Mineral.* **6**, 1-9.

SALJE, E.K.H., CROSCH, J. & EWING, R.C. (1999): Is "metamictization" of zircon a phase transition? *Am. Mineral.* (in press).

SILVER, L.T. (1991): Daughter–parent isotope systematics in U–Th-bearing igneous accessory mineral assemblages as potential indices of metamorphic history: a discussion of the concept. In *Stable Isotope Geochemistry: A Tribute to Samuel Epstein* (H.P. Taylor, Jr., J.R. O'Neil & I.R. Kaplan, eds.). The Geochemical Society, Columbus, Ohio (391-407).

SPEER, J.A. (1982a): Zircon. *In* Orthosilicates (P.H. Ribbe, ed.). *Rev. Mineral.* **5**, 67-112.

_____ (1982b): The actinide orthosilicates. *In* Orthosilicates (P.H. Ribbe, ed.). *Rev. Mineral.* **5**, 113-135.

TAYLOR, M. & EWING, R.C. (1978): The crystal structures of the ThSiO$_4$ polymorphs: huttonite and thorite. *Acta Crystallogr.* **B34**, 1074-1079.

VANCE, E.R. (1974): The anomalous optical absorption spectrum of low zircon. *Mineral. Mag.* **39**, 709-714.

_____ & ANDERSON, B.W. (1972): Study of metamict Ceylon zircons. *Mineral. Mag.* **38**, 605- 613.

VIRK, H.S. (1995): Single activation energy model of radiation damage in solid state nuclear track detectors. *Radiat. Eff. Def. Sol.* **133**, 87-95.

WANG, LU-MIN, BIRTCHER, R.C. & EWING, R.C. (1993): Ion-irradiation-induced nano-scale polycrystallization of intermetallic and ceramic materials. *Nucl. Instrum. Methods Phys. Res.* **B80/81**, 1109-1113.

_____, CAMERON, M., WEBER, W.J., CROWLEY, K.D. & EWING, R.C. (1994): In-situ observation of radiation induced amorphization of crystals with apatite structure. *In* Hydroxyapatite and Related Materials (P.W. Brown and B. Constantz, eds.). CRC Press, London, U.K. (243-249).

_____ & EWING, R.C. (1992a): Detailed in-situ study of ion beam-induced amorphization of zircon. *Nucl. Instrum. Methods Phys. Res.* **B65**, 324-329.

_____ & _____ (1992b): Ion beam induced amorphization of complex ceramic materials – minerals. *Mater. Res. Soc. Bull.* **XVII**, 38-44.

WANG, SHI-XIN (1997): *Ion Beam Irradiation-Induced Amorphization: Nano-Scale Glass Formation by Cascade Quenching*. Ph.D. dissertation, Univ. New Mexico, Albuquerque, New Mexico.

_____, WANG, LU-MIN & EWING, R.C. (1999): Ion irradiation effects for two pyrochlore compositions. *Mater. Res. Soc., Symp. Proc.* **540** (in press).

WEBER, W.J. (1990): Radiation-induced defects and amorphization in zircon. *J. Mater. Res.* **5**, 2687- 2697.

_____, DEVANATHAN, R., MELDRUM, A., BOATNER, L.A., EWING, R.C. & WANG, LU-MIN (1999): The effect of temperature and recoil spectra on amorphization of zircon. *Mater. Res. Soc., Symp. Proc.* **540** (in press).

_____, EWING, R.C., CATLOW, C.R.A., DIAZ DE LA RUBIA, T., HOBBS, L.W., KINOSHITA, C., MATZKE, H., MOTTA, A.T., NASTASI, M.A., SALJE, E.H.K., VANCE, E.R. & ZINKLE, S.J. (1998): Radiation effects in crystalline ceramics for the immobilization of high-level nuclear waste and plutonium. *J. Mater. Res.* **13**, 1434-1484.

_____, _____ & WANG, LU-MIN (1994): The radiation-induced crystalline-to-amorphous transition in zircon. *J. Mater. Res.* **9**, 688-698.

WOODHEAD, J.A., ROSSMAN, G.R. & SILVER, L.T. (1991): The metamictization of zircon: radiation dose-dependent structural characteristics. *Am. Mineral.* **76**, 74-82.

ZEITLER, P.K. & CHAMBERLAIN, C.P. (1991): Petrogenetic and tectonic significance of young leucogranites from the northwestern Himalaya, Pakistan. *Tectonics* **10**, 729-741.

ZIEGLER, J.F. (1996): TRIM Version 96.01. IBM Research, Yorktown, N.Y.

ZINKLE, S.J. & KINOSHITA, C. (1997): Defect production in ceramics. *J. Nucl. Mater.* **251**, 200-217.

Received August 6, 1998, revised manuscript accepted February 20, 1999.